Magnetic Assembly of Nanocubes for Orientation-Dependent Photonic Responses

Zhiwei Li,[†] Mingsheng Wang,[†] Xiaoliang Zhang,[†] Dawei Wang,[†] Wenjing Xu,[†] and Yadong Yin[†]*

[†]Department of Chemistry, University of California Riverside, CA 92521 (USA).

*Corresponding Author: E-mail address: yadong.yin@ucr.edu.

ABSTRACT: Close packing is the most favorable manner in colloidal self-assembly, producing superstructures with a limited variety of spatial configurations. This challenge can be overcome by incorporating anisotropic interactions into the assembly process. Using magnetite nanocubes as the building blocks, we show that they can be magnetically assembled into one-dimensional nanochains in an edge-to-edge rather than close-packed face-to-face manner. The cubic shape of the building blocks plays a key role: it decouples the easy magnetization from any of the three geometric axes favoring close packing. Therefore, under magnetic fields, the induced competition between the long-range Zeeman coupling and the short-range dipole-dipole coupling determines the assembly of nanocubes along the [110] directions. The photonic properties of the edge-to-edge configuration are dependent on both chain orientation and viewing angle. Unlike nanosphere assemblies where the strongest diffraction occurs parallel to the chain (or field) direction, the nanocubes allow to define their long-range periodicity in the plane of a thin film while diffract light out of the plane, making it particularly useful for applications that desire to achieve structural colors of sufficient intensity in a film with a minimum thickness. For example, their unique photonic property can be taken advantage to design “magic” patterns whose rotation is perceived to be opposite to the actual rotation direction of the film. Such unusual optical effects are difficult to be reproduced by other means, thereby providing many new ways for designing novel security devices. This work reveals the enormous potential of the magnetic assembly strategy, when combined with the use of well-defined nonspherical building blocks, for controlling the spatial configurations of colloidal assemblies and exploiting their novel physical properties for intriguing applications.

KEYWORDS: magnetic assembly, nanocubes, orientation, one-dimensional, photonic crystals, diffraction.

Colloidal assembly has been developed as a reliable bottom-up approach toward the fabrication of photonic crystals with rich structural diversities and well-controlled optical properties.[1-9] In principle, the collective properties of assemblies can be tailored by not only changing the physical properties of colloidal particles but also modulating the way they “bond” in the periodic structures.[10-14] In practice, however, most current research activities only produce close-packed assemblies due to the high symmetry of interacting forces. For example, polyhedral nanocrystals with shape varying from cubes to cuboctahedra, and octahedra were predicted to assemble in a close-packed face-to-face manner.[15, 16] Similar phase behavior was also observed in the nanoscale assembly of plates and rods.[17-19] As a result, this simple phase behavior greatly hinders the advancement of colloidal assembly in preparing photonic structures with more complex configurations. Introducing forces of different symmetries represents one of the promising approaches to overcome this limitation. Specifically, this purpose can be achieved by magnetic assembly of anisotropic building blocks whose magnetization does not correspond to any of the geometric axis favoring close packing. It has been long recognized that magnetic assembly is capable of not only assembling colloidal nanoparticles into ordered structures but also manipulating the dynamic equilibrium between various forces for reversible photonic response.[20-26] These are typically achieved by balancing the magnetic attractions against various repulsive forces, like electrostatic repulsion or steric hindrance.[23, 26] Although the magnetic assembly of nanospheres[27, 28] and their applications in ink-free printing, sensors, anti-counterfeiting and rewritable pads[25, 27, 29-33] have been extensively studied, magnetic assembly of anisotropic nanoparticles has not been fully explored due to the lack of uniform building blocks and practical ways to analyze the competing interactions featuring different symmetries.

Herein, using superparamagnetic nanocubes as the building blocks, we show that their assembly under external magnetic fields does not favor close packing and therefore produces unique magnetic-field-responsive photonic nanostructures that allow active tuning of their structural colors by changing the field direction. More specifically, we show that the competing effects between long-range Zeeman coupling and short-range dipole-dipole coupling in the magnetic assembly of magnetite (Fe_3O_4) nanocubes give rise to a unique edge-to-edge rather than the common face-to-face mode. The cubic shape is found to be critical in determining the overall assembly behavior: the longest axis along the corner-to-corner direction causes favorable magnetization, while close packing in a face-to-face manner produces the strongest interparticle coupling. The unique assembly behavior not only provides a well-defined model to study the dynamic magnetic interactions between nanocubes but also offers new opportunities in tuning the structural colors of the assemblies: the optical diffraction of the 1D chain-like assemblies of the nanocubes can be tuned significantly from visible to near-infrared (NIR) region by varying the directions of magnetic fields, rather than the field strength that the nanospheres assemblies rely on in the previously demonstrated case.[8, 25] This study sheds light on the dynamic interactions between anisotropic nanoparticles, provides a reliable way to modulate magnetic forces of different symmetries and also offers new opportunities for designing unique stimuli-responsive photonic nanostructures for building novel optical devices.

To prepare uniform superparamagnetic nanocubes, we used a robust post-treatment method.[34] More specifically, Prussian Blue (PB) nanocubes with an edge length of 200 nm were synthesized according to reported method[35] and then coated with a layer of silica (~25 nm in thickness) by a typical sol-gel process, as shown in the Transmission Electron Microscopy (TEM) images in **Figures 1a** and **1b**.[36] The PB@SiO_2 was then converted into Fe_3O_4@SiO_2 by a high-temperature polyol reduction process.[34, 37, 38] As shown in **Figure 1c**, small magnetite nanocrystals with a size of about 10 nm are formed inside cubic silica shells,[34, 39] which is further confirmed by the X-ray Diffraction (XRD) patterns in **Fig. s1a and s1b**. Notably, silica coating not only maintains the cubic shapes during thermal decomposition but also provides abundant negative surface charges to balance the magnetic dipole-dipole attractions in the following assembly process.[40] The size of Fe_3O_4@SiO_2 nanocubes was 344.8 ± 53.2 nm, indicating their good uniformity and dispersibility in water (**Figure. s1c**). The crystal domain is calculated to be 8.9 nm in size by Scherrer Equation, and its consistency with the TEM observation in **Figure 1c** implies that each small nanoparticle is a single crystal. The magnetic hysteresis loop in **Figure 1d** confirms the superparamagnetic nature of the building blocks with a coercivity of 2.5 G, which is consistent with the tiny small crystal domain of the as-formed magnetite. The saturated magnetization of Fe_3O_4@SiO_2 is 32.5 emu/g and comparable to that of the superparamagnetic nanospheres that have been used for constructing magnetically responsive photonic crystals in our previous research.[28]

To facilitate the observation of the assembly behavior of Fe_3O_4@SiO_2 nanocubes under different magnetic fields, we placed a permanent magnet beneath the sample stage of a dark-field optical microscope. As shown in **Fig. s2**, before exposing to a magnetic field, the samples were well-dispersed in both water and ethanol without any apparent aggregates. Under the external magnetic field, linear chain-like structures were observed with parallel alignment to the field directions, which is similar to the assembled structures in the case of nanospheres.[29, 41, 42] However, unlike the photonic chains of nanospheres which display bright structural colors under a vertical magnetic field, the diffraction of assemblies of nanocubes was negligibly weak under the same condition.[27] In addition, the chains remained randomly orientated in ethanol after removing the magnets as the electrostatic repulsion was significantly suppressed in ethanol compared with water.[26, 43] With this unique feature, the chains were further fixed by binding the neighboring nanocubes with additional silica species produced from the hydrolysis of tetraethyl orthosilicate (TEOS) in their colloidal dispersions (See supporting information for the detailed process). TEM images in **Fig. 1e and Fig. s3** clearly show that the majority of nanocubes tend to align along [110] directions, namely edge to edge manner, with few [100] (face to face) and [111] (corner to corner) defects.

It has been well-established that magnetic nanoparticles experience a packing force (coupling between the magnetic fields and induced dipoles) as well as dipole-dipole interactions under magnetic fields.[23, 44] Basically, the magnetic coupling energy is the dot product of magnetic dipole moment ($\boldsymbol{m}$) and the field ($\boldsymbol{H}$) where it is exposed, whose first derivative defines the corresponding force in the form of $\nabla(\boldsymbol{m} \cdot \boldsymbol{H})$. For 1D photonic nanochains, it can be expressed as $F=3(1-3\cos^2\Theta)$ m^2/d^4, where d is the distance between the adjacent nanoparticles and Θ is the angle between external field directions and the lines connecting two nanoparticles. These interactions also occur in the magnetic assembly of nanocubes, but along the preferential magnetization (easy axis), i.e., the [111] crystallographic direction due to the shape anisotropy.[45] Compared to other two primary axes, [100] and [110], the easy axis connects the diagonally opposite corners and is the physically longest, which could minimize the magnetic coupling potential by aligning a maximum number of dipoles within the attractive regime ($\Theta \in [0^{o}, 54.74^{o}]$). The correlation between the easy axis and the long primary axis of anisotropic nanoparticles also exists in nano ellipsoids and plates with preferential magnetization along the longitudinal and radial directions, respectively.[46-49] In **Figure 1f**, we show the simulated magnetic field distribution of 1D chains of nanospheres and nanocubes. The magnetic flux density is the largest at corners when nanocubes align along the [111] direction, suggesting the strongest coupling between magnetic fields and the induced dipoles. To the contrary, the dipole-dipole coupling approaches the maximum in face-face configurations as evidenced by obviously stronger magnetic fields between adjacent nanocubes. Experimentally, the competition between the two magnetic interactions gives rise to [110] assembly mode due to the minimization of the overall magnetic potential.[45] Notably, based on the force equation, it can be easily concluded that the strength of Zeeman coupling and dipole-dipole coupling increases as the strength of the external magnetic field. This is mainly due to the increase in the strength of both the external magnetic fields and the induced magnetic dipole moment in individual nanocubes before they reach saturated magnetization. Therefore, the two competing forces can maintain the same order of magnitude in a broad range of field strength, which, in turn, facilitates the formation of nanocube chains with uniform orientation, good periodicity, and widely tunable structural colors. Compared with isotropic nanospheres, the shape anisotropy of nanocubes breaks the coupling symmetry of not only the Zeeman effect but also the dipole-dipole interactions. In other words, the assembly of nanocubes under a magnetic field is governed by the competing local and global forces of different symmetries, thus produces 1D chains with energy-favorable [110] assembly mode .

The specific [110] arrangements of nanocubes in 1D nanochains give rise to unique photonic properties, which are different from the cases of nanospheres. In our experiments, the z-y plane was set as the incident plane with an incident angle (α) of 30°， as illustrated in **Fig. 2a**. The diffraction was found to be highly dependent on the viewing-angle (Θ) as demonstrated in **Fig. 2b and 2c**. While the aqueous dispersion of magnetic nanocubes was gray without magnets, vivid and uniform structural colors were observed, which blue-shifted from red to orange, green, cyan and finally blue by changing the viewing angle from 20° to 70°. Further quantitative measurements indicated a quasi-linear correlation between the diffraction wavelength and viewing angle with a shift rate of ~ 6 nm per degree in diffraction wavelength. Such a dependence is theoretically confirmed by solving their collective scattering by the wave optics in COMSOL Multiphysics. As the refraction occurred at the air-water interface, the incident angle was calibrated as 48.2° (see Supporting Information for simulation parameters; **Fig. s5**). As shown in **Fig. 2d and 2e**, the diffraction predicted by solving the wave equation is quite consistent with the measurement values. More practically, we systematically studied the diffractions of 1D chains by varying the directions of magnetic fields with fixed incidence and detection angles. As shown in **Fig. 2f**, the reflection peak blue-shifted when magnetic fields were rotated from -10° to 55° as illustrated in the right panel of Fig. 2a. The measured reflection covers the whole visible spectra from 500 nm to 780 nm (**Fig. 2g**). It is worth noting that the dependence of diffraction on the field strength is not as significant as the field direction. As shown in **Fig. s6**, the tunable range by varying the field strength was much narrower (between 480 nm and 600 nm) and suffered from the broadening effect owing to the degradation of both positional and orientational orders when the magnet was far from the dispersion. To interpret the physical origin of the unique optical performance, we started with a qualitative model based on ray optics, as shown in **Fig. 2h**. The optical pathway of beams reflected by the adjacent faces is highly dependent on the reflection angle (ϴ): a larger ϴ results in a shorter optical pathway, which predicts blue-shift of diffraction peak and is consistent with the experimental observations.

The viewing-angle-dependent diffraction of nanochains assembled from magnetic nanocubes and their obvious difference compared with photonic crystals based on magnetic nanospheres are fully revealed in **Fig. s7**. When a colloidal dispersion of nanospheres was exposed to a vertical magnetic field, only green was observed along different viewing angles (**Fig. s7a**). The diffraction of photonic nanochains based on nanospheres was mainly tunable by the field strength instead of the field direction as reported in our previous work.[27, 33] The dynamic equilibrium between the electrostatic repulsion and magnetic attraction between adjacent nanospheres makes the 1D photonic structures quite susceptible to field strength: the inter-particle distance and diffraction wavelength increase when field strength decreases. In the case of magnetic nanocubes, however, a continuous redshift of the structural color occurred in their colloidal dispersion under vertical magnetic fields when the viewing angles gradually decreased (**Fig. s7b**). The geometry correlation between light incidence and diffraction is summarized in **Fig. s7c**: larger viewing angle produces shorter diffraction wavelength. These observations clearly demonstrate that light will be diffracted along different directions through the colloidal dispersion owing to the shape anisotropy of nanocubes and their preferential [110] assembly manner under external magnetic fields.

To quantitatively analyze the diffraction of the assembled chains, we simulated the light field distribution by a finite-element method (COMSOL Multiphysics). The modeling and symmetry of the assembled structure are illustrated in **Fig. s5**. An S-polarized Gauss beam is incident from the top with an incident angle of 48.2° to the chain orientation, and nanocubes are aligned along their [110] direction with a separation of 30 nm. The electric field distribution and polar plots under incident light of different wavelengths are shown in **Fig. 3**. With the incidence of a 400-nm light (**Fig. 3a**), the diffracted beam is split to the right bottom with a large angle. When the incidence wavelength increases from 400 to 800 nm, it shifts from the bottom right to the top, as shown in **Fig. 3b and 3c**. Polar plots in **Fig. 3 d to 3f** indicate that light is diffracted along 127°, 107 ° and 75 ° for incidence wavelength of 400, 600 and 800 nm, respectively. By continuously sweeping the frequency of incident beam from 400 THz (750 nm) to 800 THz (375 nm) with a step of 10 THz, the shift of diffracted beams from small to large reflection angles is dynamically shown in **Supporting Videos 1 and 2**.

Direct mapping of the split of the light field is realized by dark-field scattering. As shown in **Fig. s8**, the colloidal dispersion of Fe_3O_4@SiO_2 nanocubes was sealed in a capillary with optical beam incident along the edge of the capillary. Without a magnet, only the random scattering of individual nanocubes in the colloidal solution was observed (**Fig. 4a and 4c**). Under an external magnetic field, however, the formation of 1D nanochains induced distinct diffraction patterns with unique and continuous color strips. Two symmetric optical spectra from red to blue were observed once the magnetic field direction became parallel to light incidence (0° configuration in the middle panel of **Fig. 4b**). These observations directly confirmed the angle-dependent diffraction in our previous measurements: light with shorter wavelength will be diffracted along larger reflection angles. The spatial dispersion of diffracted light is highly dependent on the orientation of 1D nanochains. When the field direction of the magnet was switched along either counter- or clockwise direction, the diffraction patterns will shift accordingly with gradually attenuated intensity (**Fig. 4b**). Relying on the spatially resolved diffraction spectra, we can intuitively visualize the diffracted light of different colors along specific directions. Taking the 0° configuration as an example, the blue beam path was observed inside the capillary at the reflection angle of about 120°. When it decreased to 60°, the color shifted from blue to green, yellow, orange, and finally red, as suggested in **Fig. 4d**.

Comparing with nanospheres assemblies, a unique feature of the nanocube assemblies is the strong dependence of their diffraction on the chain orientation, which offers excellent opportunities for designing photonic devices with novel functionalities not achievable by other means. In our previous work, when nanospheres are magnetically assembled in a thin film, the strongest diffraction is obtained along the chain direction (the field direction) which is typically perpendicular to the film surface. Since the intensity of the diffraction increases with the repeating units of the lattice, the film has to be thick enough (typically above 500 μm) to produce an easily perceptible color contrast. This is particularly a challenge for many applications that do not allow the incorporation of thick films, for example, anti-counterfeiting in banknotes which have a total thickness of ~100 μm. On the contrary, nanocubes can be assembled in the plane of the film with sufficient repeating units or chain length to exhibit high-intensity colors that are observable from outside the plane, making them ideal candidates for this type of anti-counterfeiting applications. As an example, here, we demonstrate printing of arbitrary patterns in thin films with the in-plane alignment of the nanocube assemblies by combining dynamic magnetic assembly and photolithography. As shown in **Fig. 5a**, a mixture containing colloidal dispersion of magnetic nanocubes in ethylene glycol, acrylamide monomer, and photoinitiator was first sandwiched between a glass substrate and cover glass. A UV light was then illuminated through a photomask with pre-designed patterns while a magnetic field was applied horizontally (parallel to the cover glass surfaces). The nanochains in the uncovered areas are fixed in position, with parallel alignment to the film surfaces. The photomasks and magnets were then removed, followed by another UV exposure to polymerize the rest parts of the films. To highlight the differences between the two cases, the process of fixing nanosphere-based chains is also schematically illustrated in **Fig. 5b**. Notably, a vertical magnetic field was applied during UV exposure, which gave rise to the perpendicular orientation of nanochains to the film surfaces and thereby uniform backward diffractions.[29, 30, 41] Under light illumination to the front surface, the as-made films containing nanocube chains did not display any apparent patterns against both dark (**Fig. 5c**) and white (**Fig. 5d**) backgrounds. Upon illumination at ~ 30° from the backside, a vividly blue butterfly came into view (**Fig. 5e**). As expected, the same image could show different colors, from blue to red, depending on the viewing-angles (**Fig. s9a, s9b, and s9c**). In addition, a color gradient covering the whole visible range was observed under the illumination of a point light source due to the variation in the incident angle, as shown in **Fig. 5f**. By taking advantage of the in-plane alignment of the 1D nanocube assemblies, we were able to decrease the film thickness from the initial 1 mm to 80 μm and finally 10 μm. As shown in **Fig. 5g and 5h**, they still exhibited pre-designed patterns with vivid structural colors, clearly demonstrating their significant advantage in applications where a small thickness (micrometer scale) is preferred. As shown in **Fig. s9d and s9e**, this process was able to produce any arbitrary images and letters by simply applying a pre-designed photomask during polymerization.

The unique orientation-dependent photonic response of the nanocube assemblies allows one to create some “magic” patterns of structural colors to exhibit unusual optical effects that are not attainable using spherical building blocks, thereby offering many new opportunities for designing novel security devices. **Fig. 6** demonstrates such an example. Using a photomask with the original pattern shown in **Fig. 6a,** we fixed vertically aligned nanocubes in the black regions and horizontally aligned ones in the white regions of a polymer film. When the film was illuminated from the front and viewed against a dark background, no obvious structural color was observed as demonstrated in **Fig. 6b**. When the light was illuminated from the backside, the film displayed the hidden pattern with an orientation-dependent contrast. As shown in **Fig. 6c, s10a and s10b**, at the original orientation (0°), only the regions with vertical photonic chains (black regions in **Fig. s10a**) exhibited deep blue color, producing a positive image similar to the photomask. When the film was rotated 90° counterclockwise, the orientation of the embedded nanochains in the black and white regions in **Fig. s10c** became horizontal and vertical, respectively, and the blue colors would be observed in the white regions, which was consistent with the images shown in **Fig. 6d and s10d**. Interestingly, by comparing the printed images before and after 90° rotation, we found that the film appeared to be rotated clockwise, which was opposite to the counterclockwise rotation in reality. Similarly, when the film was further rotated counterclockwise by 180° (**Fig. 6e, s10e** and **s10f)** and 270° (**Fig. 6f, s10g,** and **s10h**), the patterns were perceived to further rotate clockwise. This optical effect is attributed to the unique orientation-dependent photonic response of the nanocube assemblies and their simultaneous change in the orientation and position when the film is rotated.

Conclusions

We report here the edge-to-edge assembly of colloidal magnetite nanocubes along their [110] direction into 1D photonic structures under external magnetic fields as driven by the minimization of the competing dipole-dipole and Zeeman coupling energies originating from the shape anisotropy. The unique structure of the assemblies enables convenient tuning of the diffraction and structural color across the whole visible range by controlling the direction of the magnetic field, allowing them to operate differently from those assembled with magnetite nanospheres which display tunable optical properties dependent primarily on the field strength. The 1D nanocube assemblies exhibit bright structural colors at broad viewing-angles owing to their nonspherical shape, making them advantageous for building unique photonic devices by fixing the long-range periodic structures within the plane of a thin film while displaying the resulting structural colors out of the plane. This is a beneficial feature for many applications, such as anti-counterfeiting, where it is desirable to produce a structural color of sufficient intensity in a film having a minimum thickness. With the assistance of photolithography, we further demonstrate that predesigned patterns can be encrypted in a thin polymer film by controlling the orientation of the nanocube assemblies at designated locations. The encrypted patterns can only be observed by orienting them along a certain direction or by exposing them to light incident from a particular angle. Further, the unique orientation-dependent photonic response of the nanocube assemblies can be employed to create "magic" patterns whose rotation is perceived to be opposite to the actual rotation direction of the film. Such unusual optical effects are not achievable using nanosphere assemblies and are not easily cloned by other fabrication methods, thereby providing many new ways for designing novel security devices. We believe this work highlights that the magnetic assembly strategy, when applied to nonspherical colloidal building blocks, can offer abundant opportunities in producing unique superstructures that can display interesting photonic properties.

ASSOCIATED CONTENT

Supporting Information

Experimental details, TEM images, XRD patterns, reflection spectra, optical microscope images, digital photographs and simulations results including Figures S1-S10 (PDF).

AUTHOR INFORMATION

Corresponding Author

*E-mail: yadong.yin@ucr.edu.

ORCID

Zhiwei Li: 0000-0002-1489-4506

Yadong Yin: 0000-0003-0218-3042

Author Contributions

Li and Yin conceived and designed the experiments. Li performed the experiments. Wang, Zhang, Wang, Xu and Li contributed to result analysis. Li and Yin analyzed the results and wrote the manuscript. All authors have given approval to the final version of the manuscript.

Notes

The authors declare no competing financial interest.

ACKNOWLEDGMENT

This work was supported by the U.S. National Science Foundation (DMR-1810485).

REFERENCES

1. Li, F.; Josephson, D. P.; Stein, A. *Angew. Chem. Int. Ed.* **2011,** 50, 360-388.
2. Whitesides, G. M.; Grzybowski, B. *Science* **2002,** 295, 2418-2421.
3. Yin, Y.; Lu, Y.; Gates, B.; Xia, Y. *J. Am. Chem. Soc.* **2001,** 123, 8718-8729.
4. Xia, Y.; Yin, Y.; Lu, Y.; McLellan, J. *Adv. Funct. Mater.* **2003,** 13, 907-918.
5. Ozin, G. A.; Yang, S. M. *Adv. Funct. Mater.* **2001,** 11, 95-104.
6. Lu, Y.; Yin, Y.; Xia, Y. *Adv. Mater.* **2001,** 13, 415-420.
7. Yin, Y.; Xia, Y. *Adv. Mater.* **2001,** 13, 267-271.
8. Ge, J.; Hu, Y.; Yin, Y. *Angew. Chem. Int. Ed.* **2007,** 46, 7428-7431.
9. Wang, Y.; Cui, H.; Zhao, Q.; Du, X. *Matter* **2019,** 1, 1-13.
10. Zhang, Q.; Janner, M.; He, L.; Wang, M.; Hu, Y.; Lu, Y.; Yin, Y. *Nano Lett.* **2013,** 13, 1770-1775.
11. Batista, C. A. S.; Larson, R. G.; Kotov, N. A. *Science* **2015,** 350, 1242477.
12. Li, Z.; Yin, Y. *Adv. Mater.* **2019,** 31, 1807061.
13. Li, Z.; Yang, F.; Yin, Y. *Adv. Funct. Mater.* **2019,** 1903467.

14. Singh, G.; Chan, H.; Baskin, A.; Gelman, E.; Repnin, N.; Král, P.; Klajn, R. *Science* **2014,** 345, 1149-1153.
15. Henzie, J.; Grünwald, M.; Widmer-Cooper, A.; Geissler, P. L.; Yang, P. *Nature Mater.* **2012,** 11, 131.
16. Damasceno, P. F.; Engel, M.; Glotzer, S. C. *Science* **2012,** 337, 453-457.
17. Li, P.; Li, Y.; Zhou, Z. K.; Tang, S.; Yu, X. F.; Xiao, S.; Wu, Z.; Xiao, Q.; Zhao, Y.; Wang, H. *Adv. Mater.* **2016,** 28, 2511-2517.
18. Murphy, C. J.; Sau, T. K.; Gole, A. M.; Orendorff, C. J.; Gao, J.; Gou, L.; Hunyadi, S. E.; Li, T., *J. Phys. Chem. B*, **2005**, 109, (29), 13857-13870.
19. Li, H.; Li, C.; Sun, W.; Wang, Y.; Hua, W.; Liu, J.; Zhang, S.; Chen, Z.; Wang, S.; Wu, Z. *Adv. Mater.* **2019,** 31, 1900388.
20. Xu, X.; Friedman, G.; Humfeld, K. D.; Majetich, S. A.; Asher, S. A. *Adv. Mater.* **2001,** 13, 1681-1684.
21. Erb, R. M.; Son, H. S.; Samanta, B.; Rotello, V. M.; Yellen, B. B. *Nature* **2009,** 457, 999.
22. Gates, B.; Xia, Y. *Adv. Mater.* **2001,** 13, 1605-1608.
23. He, L.; Wang, M.; Ge, J.; Yin, Y. *Acc. Chem. Res.* **2012,** 45, 1431-1440.
24. He, L.; Hu, Y.; Kim, H.; Ge, J.; Kwon, S.; Yin, Y. *Nano Lett.* **2010,** 10, 4708-4714.
25. Ge, J.; Yin, Y. *Angew. Chem. Int. Ed.* **2011,** 50, 1492-1522.
26. Ge, J.; He, L.; Goebl, J.; Yin, Y. *J. Am. Chem. Soc.* **2009,** 131, 3484-3486.
27. Ge, J.; Hu, Y.; Yin, Y. *Angewandte Chemie* **2007,** 119, 7572-7575.
28. Ge, J.; Hu, Y.; Biasini, M.; Beyermann, W. P.; Yin, Y. *Angew. Chem. Int. Ed.* **2007,** 46, 4342-4345.
29. Ge, J.; Lee, H.; He, L.; Kim, J.; Lu, Z.; Kim, H.; Goebl, J.; Kwon, S.; Yin, Y. *J. Am. Chem. Soc.* **2009,** 131, 15687-15694.
30. Ge, J.; Goebl, J.; He, L.; Lu, Z.; Yin, Y. *Adv. Mater.* **2009,** 21, 4259-4264.
31. Xuan, R.; Wu, Q.; Yin, Y.; Ge, J. *J. Mater. Chem.* **2011,** 21, 3672-3676.
32. Zhao, Q.; Wang, Y.; Cui, H.; Du, X. *J. Mater. Chem. C* **2019,** 7, 6493-6511.
33. Kim, H.; Ge, J.; Kim, J.; Choi, S.-e.; Lee, H.; Lee, H.; Park, W.; Yin, Y.; Kwon, S. *Nature Photon.* **2009,** 3, 534.
34. Xu, W.; Wang, M.; Li, Z.; Wang, X.; Wang, Y.; Xing, M.; Yin, Y. *Nano Lett.* **2017,** 17, 2713-2718.
35. Hu, M.; Furukawa, S.; Ohtani, R.; Sukegawa, H.; Nemoto, Y.; Reboul, J.; Kitagawa, S.; Yamauchi, Y. *Angewandte Chemie* **2012,** 124, 1008-1012.
36. Lu, Y.; Yin, Y.; Mayers, B. T.; Xia, Y. *Nano Lett.* **2002,** 2, 183-186.
37. Sun, Y.; Xia, Y. *Adv. Mater.* **2002,** 14, 833-837.
38. Sun, Y.; Xia, Y. *Science* **2002,** 298, 2176-2179.
39. Hu, M.; Belik, A. A.; Imura, M.; Mibu, K.; Tsujimoto, Y.; Yamauchi, Y. *Chem. Mater.* **2012,** 24, 2698-2707.
40. Wang, M.; He, L.; Xu, W.; Wang, X.; Yin, Y. *Angew. Chem. Int. Ed.* **2015,** 54, 7077-7081.
41. Hu, Y.; He, L.; Yin, Y. *Angew. Chem. Int. Ed.* **2011,** 50, 3747-3750.
42. Wang, M.; He, L.; Hu, Y.; Yin, Y. *J. Mater. Chem. C* **2013,** 1, 6151-6156.
43. Ge, J.; Yin, Y. *Adv. Mater.* **2008,** 20, 3485-3491.
44. Ge, J.; He, L.; Hu, Y.; Yin, Y. *Nanoscale* **2011,** 3, 177-183.
45. Singh, G.; Chan, H.; Baskin, A.; Gelman, E.; Repnin, N.; Král, P.; Klajn, R. *Science* **2014,** 1254132.
46. Wang, M.; He, L.; Zorba, S.; Yin, Y. *Nano Lett.* **2014,** 14, 3966-3971.

47. Wang, M.; Gao, C.; He, L.; Lu, Q.; Zhang, J.; Tang, C.; Zorba, S.; Yin, Y. *J. Am. Chem. Soc.* **2013,** 135, 15302-15305.
48. Mao, Y.; Liu, J.; Ge, J. *Langmuir* **2012,** 28, 13112-13117.
49. Bubenhofer, S.; Athanassiou, E.; Grass, R.; Koehler, F.; Rossier, M.; Stark, W. J. *Nanotechnology* **2009,** 20, 485302.

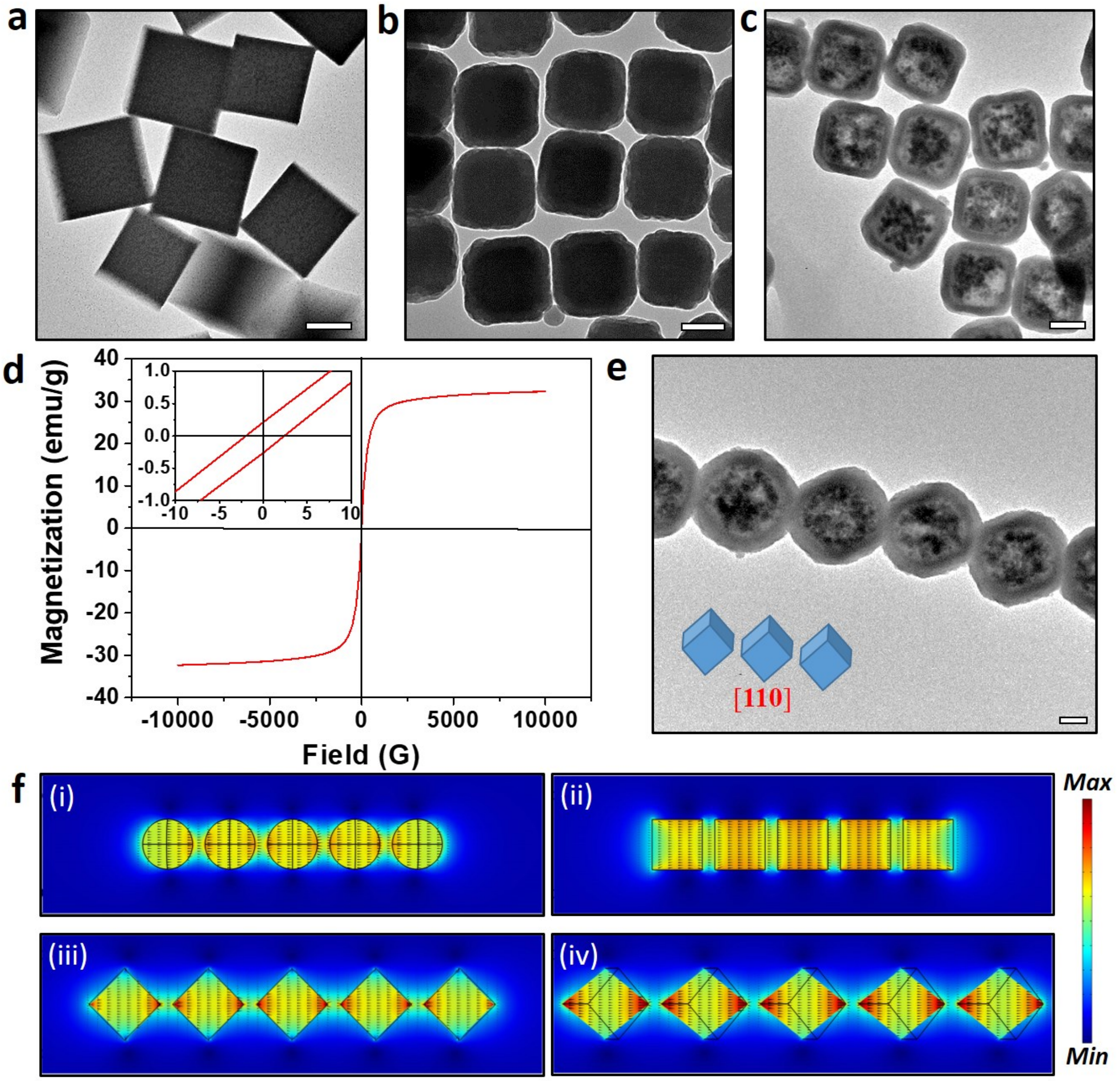

Figure 1. TEM images of (**a**) PB, (**b**) PB@SiO_2 and (**c**) Fe_3O_4@SiO_2 nanocubes. (**d**) Magnetic hysteresis loop of the Fe_3O_4@SiO_2. Inset: expanded low-field curve. (**e**) TEM image of assembled 1D chain-like structures fixed by additional silica coating. (**f**) Simulated magnetic field distribution of various chains of (i) nanospheres, and nanocubes assembled along the (ii) [100], (iii) [110] and (iv) [111] directions. Scale bars: 100 nm.

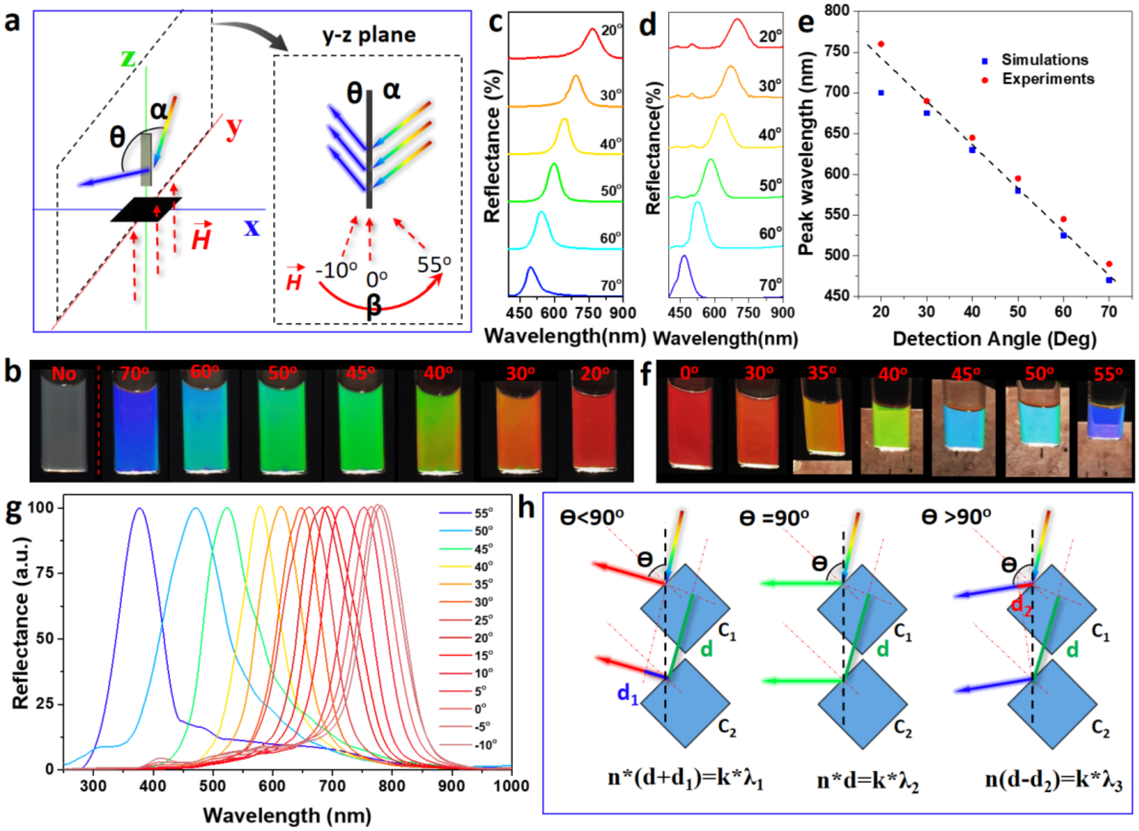

Figure 2. (**a**) Schematic illustration of the geometry for optical measurements. (**b**) Optical images of a colloidal dispersion of Fe_3O_4@SiO_2 nanocubes in capillary without and with magnetic field under different viewing angles. Reflection spectra measured (**c**) and simulated (**d**) at different viewing angles (ϴ). The incident angle, α, is set at 30°. (**e**) The correlation between the peak position of reflection and detection angles. (**f**) Optical images of colloidal dispersions of Fe_3O_4@SiO_2 nanocubes in capillary under various directions (β) of magnetic fields as illustrated in the right panel of Fig. 2a. Note that the capillaries in the images were tilted slightly to get uniform structural colors in the colloidal dispersions. (**g**) The corresponding normalized reflection spectra measured by varying the directions of the external magnetic field (β). (**h**) Qualitative ray-optic model predicting the difference of light pathway along three typical directions.

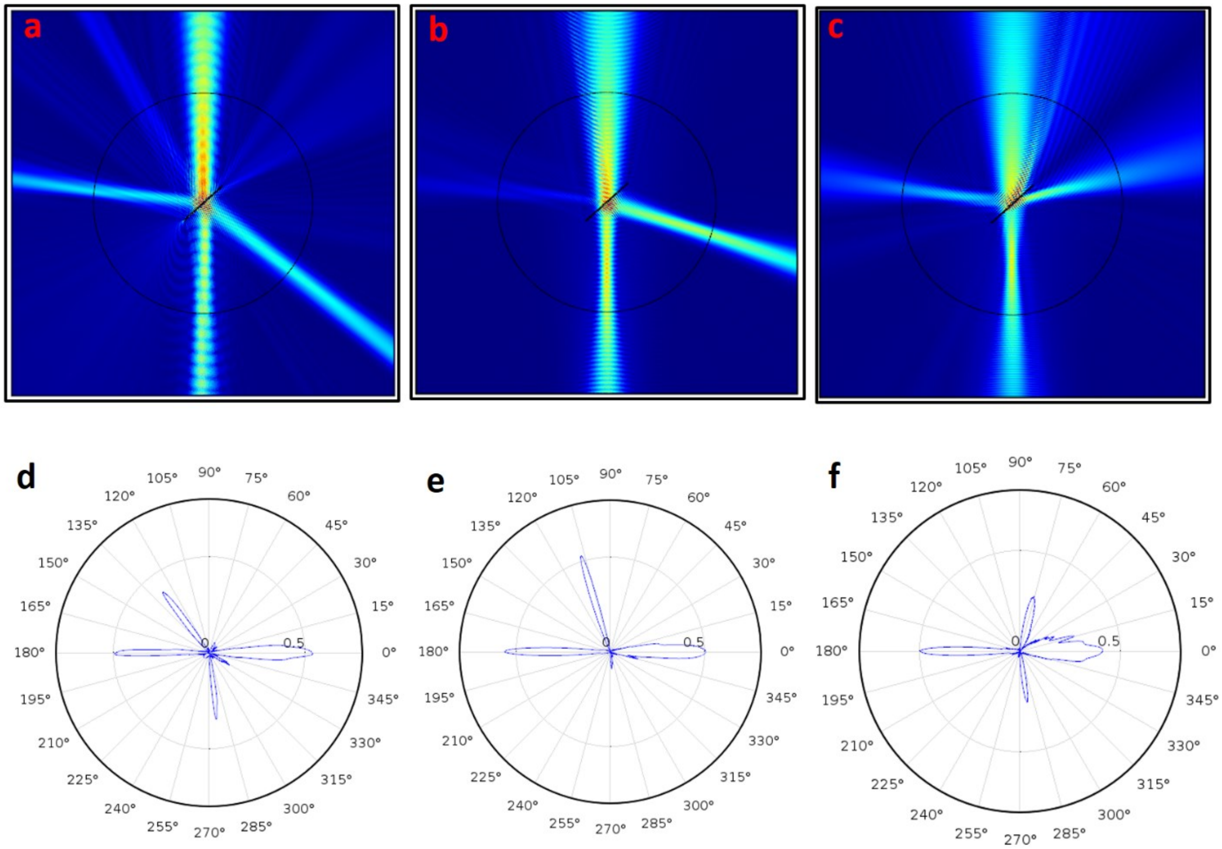

Figure 3. Electric field distributions under incident light with wavelengths of (**a**) 400 nm, (**b**) 600 nm and (**c**) 800 nm. (**d**), (**e**) and (**f**) The corresponding polar plots.

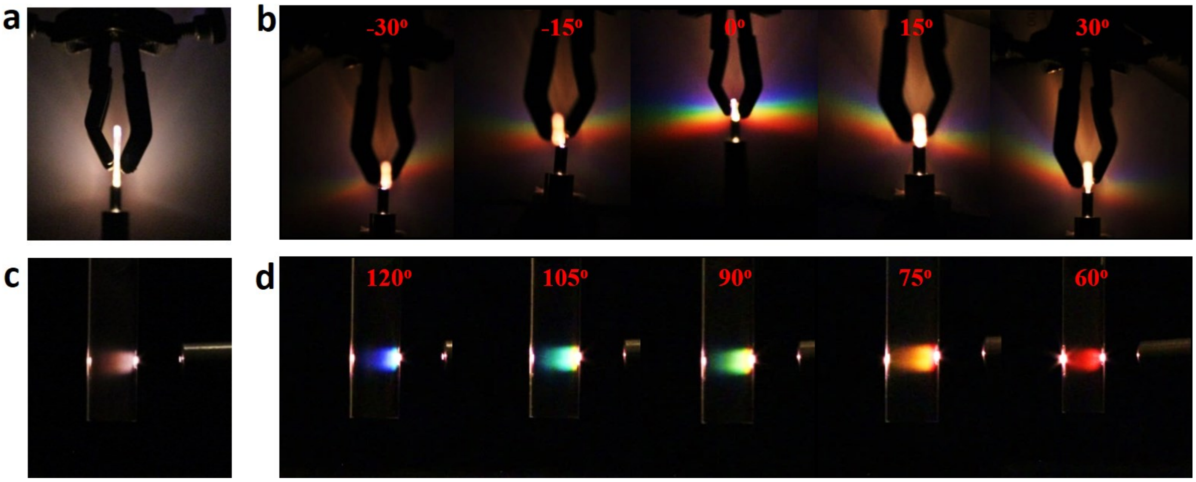

Figure 4. (**a**) Optical image of light scattered by colloidal dispersion without magnetic field. (**b**) Optical images of light scattered under different orientations of magnetic fields. (**c**) Side view of colloidal dispersion in capillary without magnetic field. (**d**) Side views of colloidal dispersion with magnetic field under different viewing angles (Ө).

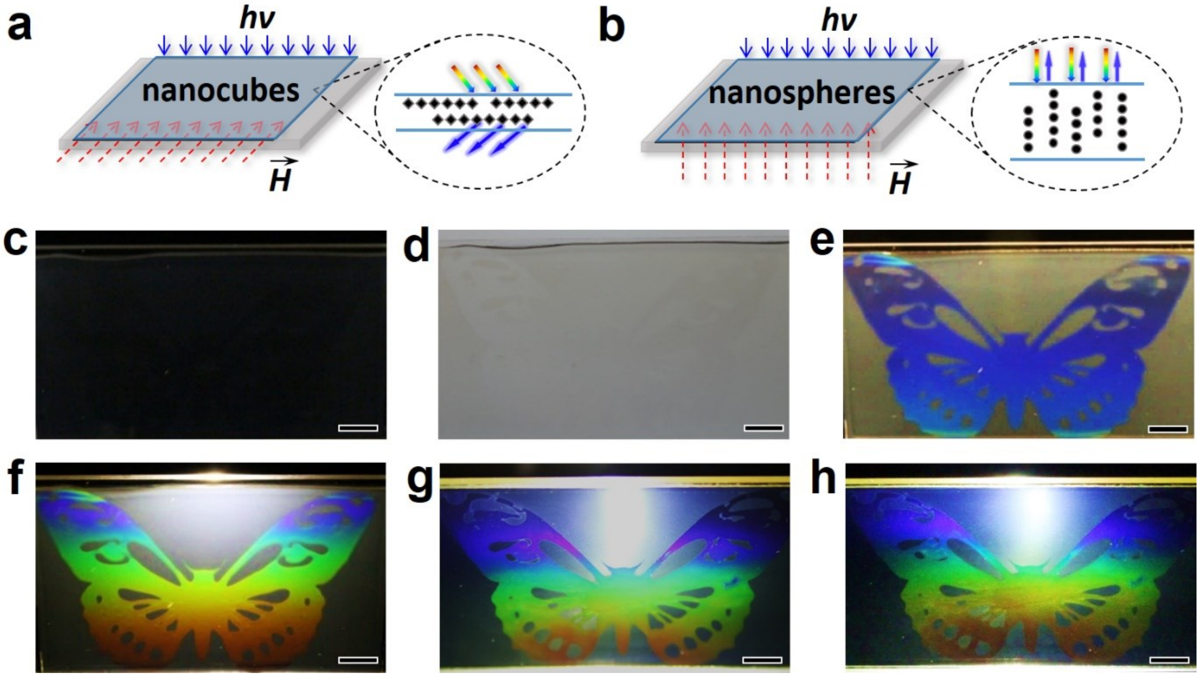

Figure 5. (**a, b**) Scheme showing the directional setting for fixing the (a) nanocube and (b) nanosphere assemblies in a thin film. The nanocube chains are parallel to the surface of the film so that light diffracts out of plain, while the nanosphere chains are perpendicular to the film surface and light diffracts backward. (**c, d**) Optical images of the film containing nanocubes taken against a (**c**) dark and (**d**) bright background, with the light illuminating from the front. (**e**) The same film under directional light illumination at ~ 30º from the backside. (**f-h**) Films of different thicknesses under the illumination of a point light source: 1 mm (**f**), 80 µm (**g**), and 10 µm (**h**). Scale bars: 5 mm.

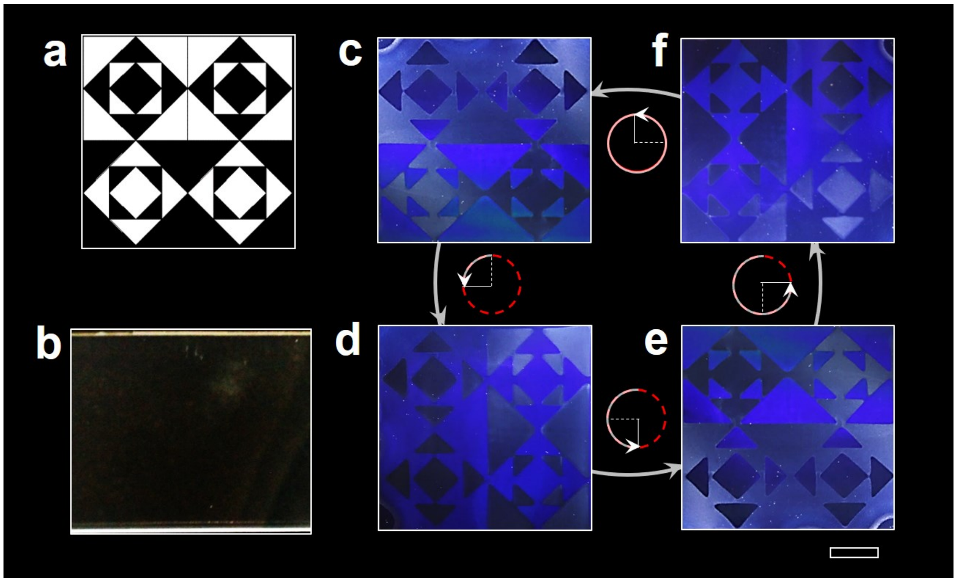

Figure 6. (**a**) Photomask used for printing an encryption film. The nanocube chains were fixed with a vertical and horizontal orientation in the dark and white regions, respectively. (**b**) Digital images of the printed pattern taken against a dark background. (**c-f**) Digital images of the printed pattern under the same light illumination but with counterclockwise rotation from (**c**) 0° to (**d**) 90°, (**e**) 180° and (**f**) 270°. The pattern rotates counterclockwise, but it appears to rotate clockwise. Scale bar: 5 mm.

TOC graphic

Magnetic Assembly of Nanocubes for Orientation-Dependent Photonic Responses